Flux jumps in melt-textured Y-Ba-Cu-O

K.-H. Müller and C. Andrikidis
CSIRO, Division of Applied Physics, Lindfield, Australia 2070
(Received 6 July 1993; revised manuscript received 4 October 1993)

The magnetization of a melt-textured Y-Ba-Cu-O superconducting sample has been measured in magnetic fields up to 5.5 T using a SQUID magnetometer. Partial flux jumps were observed below the temperature of 7.6 K. With the applied field parallel to the sample's c axis, the upper bound of the instability field was found to be the maximum applied field, while with the applied field perpendicular to the c axis, the sample's dimensions determined the upper bound. Magnetization loops with flux jumps were calculated employing a critical-state model which incorporates the flux-jump instability criterion and considers the incompleteness of jumps. The different shapes of the magnetization loops are determined by four model parameters of which the instability field of the first virgin jump has the strongest effect on the loop shape. To predict the observed loop asymmetry and the appearance of solitary jumps, the simple Bean critical-state model was found to be insufficient. Instead, a critical-state model where the critical current density decreases as a function of the magnetic field is needed. It is shown that the use of a simple Kim-type critical current density is adequate to explain in detail all our experimental flux-jump data.

I. INTRODUCTION

As the applied field acting on a type-II superconductor is increased beyond the instability field, H_{fi}, it is possible for a disturbance cycle to become initiated that leads to a macroscopic ingress of flux usually referred to as flux jump.[1,2] Flux jumps have been studied extensively in conventional type-II superconductors; in particular, in connection with wires and magnetic coils, where the appearance of magnetic instabilities is avoided by decreasing the diameter of the superconductor, i.e., introducing wires of multifilamentary structure.[3] Since the discovery of the high-temperature superconductors (HTS), flux jumps have been observed[4] in large single crystals of Y-Ba-Cu-O (Refs. 5 and 6), Ho-Ba-Cu-O (Ref. 7), and Bi-Sr-Ca-Cu-O (Ref. 8) as well as in melt-textured Y-Ba-Cu-O.[9–12] In all of these cases the samples possessed a very high transport critical current density without the apparent weak links.

Magnetic stability predictions for HTS have been made ever since the necessary parameters became available,[13–18] which are the critical temperature T_c and the specific heat C_v. Because of the high T_c and large specific heat C_v of HTS, the instability field H_{fi} is much larger than in conventional superconductors. The calculated instability field (under adiabatic conditions) reaches a maximum value of about $\mu_0 H_{fi}=8$ T at a temperature of about 50 K for the Y-Ba-Cu-O superconductor and a maximum value of $\mu_0 H_{fi}=14$ T at about 90 K for the Tl-Ba-Cu-O material[4] while for conventional superconductors the maximum is only about 0.4 T. Because of the large instability field in HTS, a multifilamentary structure in wires or tapes has become a far less stringent requirement.[14,18] Furthermore, because of the large instability fields, a strong field can be trapped and the old concept of producing superconducting permanent magnets might become applicable.[19,20]

Flux jumps in type-II superconductors can be observed by measuring the magnetization.[4] In this paper we report on measurements and calculations of magnetization loops with flux jumps for a melt-textured Y-Ba-Cu-O superconducting sample in fields up to 5.5 T. Magnetization loops with solitary flux jumps and jumps in the virgin magnetization curve were calculated in detail by employing a critical state model and using the instability field concept introduced by Wipf[1] and Schwarz and Bean.[2] It is shown that in order to explain quantitatively the magnetization loops with solitary jumps and to predict the observed asymmetry between the upper and lower magnetization branches, the Bean critical-state model is not sufficient but instead a critical-state model which makes use of a critical current density that decreases in a magnetic field needs to be employed. In the model the rather complex shape of the magnetization loop is characterized by only four parameters. Slight changes in one of these parameters, i.e., the value of the instability field, H_{fi}, is shown to cause dramatic changes in the magnetization loop.

II. EXPERIMENT

The Y-Ba-Cu-O sample was prepared by the conventional solid-state reaction and melt-textured growth process.[21] Compared with the sintered Y-Ba-Cu-O material, the melt-textured samples have a much higher critical current density J_c due to the elimination of grain boundary weak links. The dimensions of the sample were $a_x=1.9$ mm, $a_y=1.7$ mm, and $a_z=1.3$ mm where the crystallographic c direction was along the z axis. The base and one side of the sample were glued to a vertical step made out of Perspex and the sample was then mounted into a commercial Quantum Design SQUID magnetometer. Here the sample was zero-field cooled to the measuring temperature which varied between 2 and 90 K. The magnetization was measured for an increasing

applied field from 0 to 5.5 T (virgin magnetization curve), then for a decreasing field from 5.5 to −5.5 T (upper magnetization branch) and finally for a field from −5.5 to 5.5 T (lower magnetization branch). The sweep rate of the applied field was 1.2 T/min and the sweep was paused for 5 s before each magnetic moment measurement which took 10 s. Contrary to the observation in Ref. 10, no dependence of the magnetization on the pause (0–150 s) could be found which we think is due to the more adiabatic condition for our sample. Measurements were performed with the c axis of the sample parallel and perpendicular to the applied field.

III. THEORETICAL MODEL WITH FLUX JUMPS

A. Critical state

We assume that the critical current density $J_c(H)$ is of Kim-type,[22] thus

$$J_c(T,H)=J_0(T)\frac{H_0(T)}{H_0(T)+|H|}\ , \tag{1}$$

where H_0 is a phenomenological parameter and J_0 the critical current density at zero magnetic field. Both J_0 and H_0 depend on temperature T.

The magnetic field inside a type-II superconductor is arranged in such a way that everywhere in the superconductor the Lorentz force density is balanced by the pinning force density. Under such conditions the magnetic field inside is said to be in a critical state. Instead of a cubic sample like ours, let us consider for simplicity a sample in the form of an infinite slab of thickness d where the external magnetic field H_a is applied parallel to the slab. The magnetic field profile $H(x)$ inside the sample is then given by the solutions of the critical-state equation

$$\frac{dH}{dx}=\begin{cases}\pm J_c[H(x)] & \text{in regions penetrated by the field}\\ 0 & \text{otherwise}\ ,\end{cases} \tag{2}$$

where the boundary condition is $H_a=H(x=0)=H(x=d)$. The $\pm$ signs correspond to domains of x where vortices have moved into or out of the type-II superconductor. The above critical-state equation [Eq. (2)] assumes that $B=\mu_0 H$ and can be used for determining the magnetization as long as the magnetic fields involved are much greater than the lower critical field, H_{c1}.[23,24] Because the magnetic field used to investigate flux jumps in magnetization loops of melt-textured Y-Ba-Cu-O are several Tesla and thus much greater than H_{c1}, which is in the order of several hundred Gauss at $T=0$,[25] the simple Eq. (2) can be applied. The extent to which the magnetization of a slab approximates that of a cube shall be discussed below.

The different solutions of Eq. (2) for a semi-infinite slab ($d\rightarrow\infty$) are

$$\text{(i)}\quad H(x)=-H_0+\sqrt{(H_0+H_a)^2+2J_0H_0x} \tag{3}$$

for flux lines moving out of the superconductor [see curve (1) in Fig. 1(a)] and

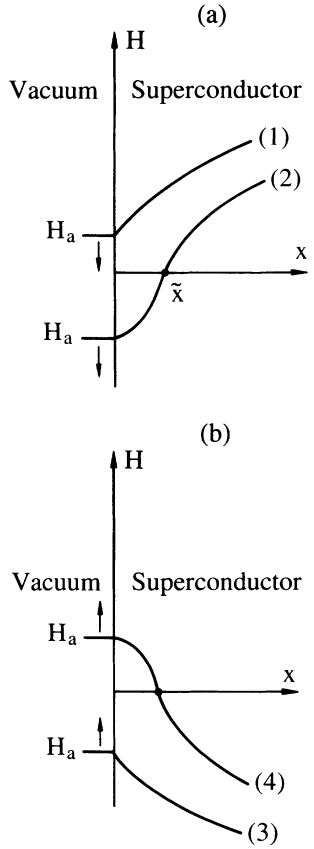

FIG. 1. Solutions of the critical-state equation [Eq. (2)] for a semi-infinite slab (a) for a decreasing applied field H_a and (b) for an increasing applied field H_a.

$$\text{(ii)}\quad H(x)=H_0-\sqrt{(H_0-H_a)^2-2J_0H_0x}$$
$$\text{for } 0\le x\le\bar{x}\ , \tag{4}$$

$$H(x)=-H_0+\sqrt{H_0^2+2J_0H_0(x-\bar{x})}\quad \text{for } \bar{x}\le x\ , \tag{5}$$

where

$$\bar{x}=\frac{(H_0-H_a)^2-H_0^2}{2J_0H_0} \tag{6}$$

for antiflux lines moving into the superconductor [see curve (2) in Fig. 1(a)]. Figure 1(b) represents two further solutions of Eq. (2) which can be obtained from Eqs. (3)–(6) by replacing $H(x)$ by $-H(x)$ and H_a by $-H_a$. It is important to notice that from these four solutions all possible magnetic field profiles for a slab of *finite* thickness d can be constructed as long as flux jumps do not occur. If a flux jump occurs the temperature in the sample increases for a short time due to the ingress of flux lines. A new magnetic field profile which corresponds to a critical current density, J_{0j}, is established, where $J_{0j}<J_0$. Shortly after the jump has taken place the temperature drops back to the bath (measuring) temperature and the profile is frozen-in. The field profile after the jump can be constructed from the above mentioned four solutions where now J_{0j} instead of J_0 is used in Eqs.

(3)–(6). From these eight solutions all the necessary magnetic field profiles required to calculate magnetization loops with flux jumps can be constructed.

B. Flux jumps, instability criterion, and magnetization loop

Magnetic flux jumps can occur for quite different magnetic field profiles inside a superconductor. Figure 2(a) shows the different field profiles with jumps used to determine the virgin magnetization while Fig. 2(b) displays field profiles with jumps used to determine the upper branch of the magnetization loop. In Fig. 2 it is assumed that each jump is incomplete and that the maximum temperature reached during a jump, which is less than T_c, is the same for all jumps.

The instability criterion for flux jumps in the case of a Kim-type critical current density $J_c(H)$ [Eq. (1)] is derived similarly as in the case of a Bean-type J_c where J_c is independent of H. If the applied field H_a increases by a small amount ΔH_a ($\Delta H_a \ll H_a$) flux lines move into the type-II superconductor. Due to the ingress of flux lines, the magnetic field increases by $\Delta H(x)$ (see Fig. 3) and the

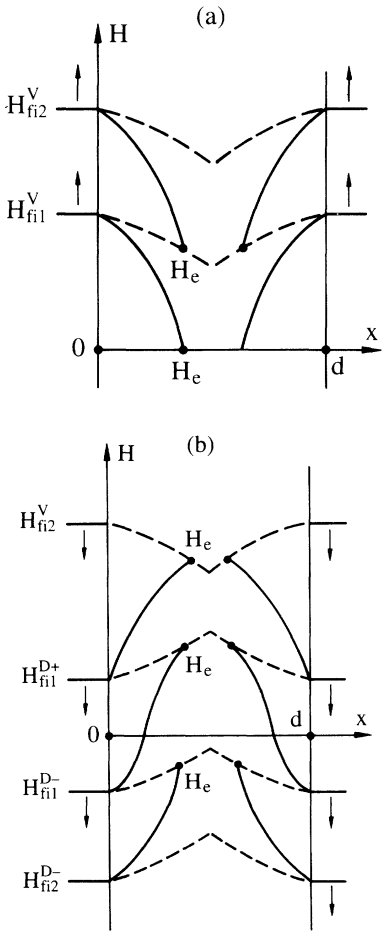

FIG. 2. Magnetic-field profile $H(x)$ inside a slab of thickness d. The dashed curves represent the magnetic-field distribution after a flux jump. (a) Virgin magnetic field profiles with jumps at H^V_{fi1} and H^V_{fi2}. (b) Magnetic-field profiles in a decreasing applied magnetic field with jumps at H^{D+}_{fi1}, H^{D-}_{fi1}, and H^{D-}_{fi2}.

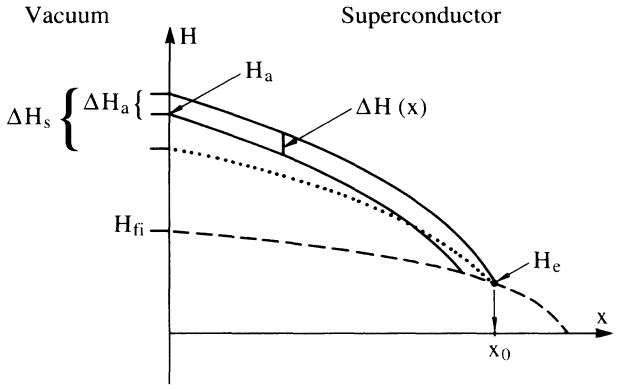

FIG. 3. Magnetic-field distribution $H(x)$ in a semi-infinite slab where the field has been increased after a jump from H_{fi} to H_a. The increase of the applied field by $\Delta H(x)$ raises the temperature such that the shielded field drops by ΔH_s (dotted curve).

energy Q per unit volume is dissipated in the vicinity of x where

$$Q(x)=\mu_0 J_c(x)\int_x^{x_0}\Delta H(x')dx' \ . \tag{7}$$

Because in the HTS materials the electromagnetic diffusivity D_n is much greater than the thermal diffusivity $D_{\rm th}$ the short lasting fluctuation ΔH_a causes a sudden rise in temperature at x by ΔT. Under local adiabatic conditions one obtains

$$\Delta T(x)=Q(x)/C_v \ , \tag{8}$$

where C_v is the specific heat of the superconductor. The temperature rise reduces the critical current by ΔJ_c where

$$\Delta J_c(x)=\frac{\partial J_c}{\partial T}\Delta T(x) \ . \tag{9}$$

The reduction in J_c weakens the shielding ability of the superconductor by ΔH_s (see Fig. 3), where

$$\Delta H_s=-\int_0^{x_0}\Delta J_c(x')dx' \quad \text{(Maxwell's equation)} \tag{10}$$

and the magnetic-field configuration is unstable with respect to a flux jump if $\Delta H_s > \Delta H_a$.

From Eqs. (7)–(10) one obtains

$$\Delta H_s=-\int_0^{x_0}\frac{\partial J_c(x')}{\partial T}\frac{\mu_0 J_c(x')}{C_v}\int_{x'}^{x_0}\Delta H(x'')dx''dx' \ . \tag{11}$$

In the case that a flux jump occurs in the virgin magnetization [Fig. 2(a)] one finds for $\Delta H(x'')$ using Eq. (4) and replacing $H(x)$ by $-H(x)$ and H_a by $-H_a$

$$\Delta H(x'')=\frac{(H_0+H_a)\Delta H_a}{[(H_0+H_a)^2-2J_0H_0x'']^{1/2}} \ . \tag{12}$$

Employing Eqs. (11) and (12) and assuming that $H_0(T)$ does not vary much with T at the temperature of interest,

one derives for the instability field, H_{fi}, using the criterion $\Delta H_s = \Delta H_a$

$$2\left[(|H_{fi}|-|H_e|)(|H_{fi}|+H_0)+(|H_{fi}|+H_0)(|H_e|+H_0)\ln\frac{H_0+|H_e|}{H_0+|H_{fi}|}\right]=\frac{2C_vJ_0}{\mu_0(-\partial J_0/\partial T)}=H_{j0}^2 . \quad (13)$$

The above equation also defines the quantity H_{j0}. For the first virgin jump the field H_e is equal to zero and for further jumps H_e is greater than zero [Fig. 2(a)]. The absolute values of H_{fi} and H_e are introduced in Eq. (13) to include the case where $H_{fi}<0$ and $H_e<0$ [see Fig. 2(b) where $H_a=H_{fi}=H_{fi2}^{D-}$].

In the limit $H_0\to\infty$ (Bean-type J_c), Eq. (13) becomes

$$H_{fi}=\left[\frac{2C_vJ_0}{\mu_0(-\partial J_0/\partial T)}\right]^{1/2}=H_{j0} , \quad (14)$$

which is a commonly used expression[26] to estimate the instability field H_{fi}.

Using the fact that in HTS materials $J_0(T)\simeq J_0(0)(1-T/T_c)$ one obtains

$$H_{j0}=\sqrt{2\mu_0^{-1}C_v(T)(T_c-T)} . \quad (15)$$

In the case that a flux jump occurs when the applied field H_a is decreased but still positive [see Fig. 2(b) where $H_a=H_{fi}=H_{fi1}^{D+}$] one derives from Eq. (3)

$$\Delta H(x'')=\frac{(H_0+H_a)\Delta H_a}{[(H_0+H_a)^2+2J_0H_0x'']^{1/2}} . \quad (16)$$

Employing Eqs. (11) and (16) results again in Eq. (13) for the instability field, H_{fi}.

In the case that a jump occurs when the applied field is negative and $H_e>0$ [jump at $H_a=H_{fi}=H_{fi1}^{D-}$ in Fig. 2(b)] one derives from Eq. (4)

$$\Delta H(x'')=\frac{(H_0-H_a)\Delta H_a}{[(H_0-H_a)^2-2J_0H_0x'']^{1/2}} \quad \text{for } 0\le x''\le\tilde{x} , \quad (17)$$

where $\tilde{x}$ is given by Eq. (6), and from Eq. (5)

$$\Delta H(x'')=\frac{(H_0-H_a)\Delta H_a}{[2H_0^2-(H_0-H_a)^2+2J_0H_0x'']^{1/2}} \quad \text{for } \tilde{x}<x'' . \quad (18)$$

Substituting the above expressions for $\Delta H(x'')$ into Eq. (11) and assuming that $H_0(T)$ does not vary much with T at the temperature of interest, one finds for the instability field, H_{fi},

$$2(H_0+|H_{fi}|)\left[(|H_e|-H_0)\ln\frac{H_0+|H_{fi}|}{H_0}+(|H_e|+H_0)\ln\frac{H_0+|H_e|}{H_0}+|H_{fi}|-|H_e|\right]=\frac{2J_0C_v}{\mu_0(-\partial J_0/\partial T)}=H_{j0}^2 . \quad (19)$$

The absolute values of H_{fi} and H_e are introduced in Eq. (19) to include the case where $H_{fi}>0$ and $H_e<0$ (lower magnetization branch). In order to calculate the magnetization when the applied field H_a is swept between the maximum field H_m and the largest negative field $-H_m$ it is useful to distinguish between three different types of magnetization loops.

(i) The magnetization loop which contains solitary jumps. Here no jump appears in the virgin magnetization and only one jump occurs in the upper branch and one in the lower branch of the magnetization loop.

(ii) The magnetization loop which shows a single jump in the virgin magnetization curve, no jump when the field is swept from H_m to 0 and a single jump (or several jumps) between 0 and $-H_m$, and similarly for the lower branch.

(iii) The magnetization loop which shows at least one jump in the virgin magnetization curve, one or several jumps when the field is swept from H_m to 0 and further jumps between 0 and $-H_m$, and similar for the lower branch of the magnetization.

These three different classes of loops require a separate mathematical analysis because of differences in the magnetic field profiles, $H(x)$. The profiles can be constructed from the eight different solutions of Eq. (2) some of which are given by Eqs. (3)–(5). The instability field H_{fi} can be calculated using Eqs. (13) and (19) where the value of the field H_e depends on the magnetic history of the sample. From the analytical expressions of the magnetic-field profiles $H(x)$, the magnetization M can be calculated as a function of H_a. For a slab of thickness d

$$M=\frac{2}{d}\int_0^{d/2}H(x)dx-H_a . \quad (20)$$

Analytical expressions of the magnetization M for case (i) i.e., solitary jumps are given in the Appendix. The analytical expressions of M for the cases (ii) and (iii) are not given here because of their length but they are similar to the ones in the Appendix and can be derived easily following the procedure outlined there.

IV. RESULTS AND DISCUSSION

Figures 4(a)–4(e) show the measured magnetization loops at temperatures between 2.5 and 7.75 K where the field is applied parallel to the crystallographic c axis of the melt-textured Y-Ba-Cu-O sample. Due to the appearance of flux jumps and their strong dependence on temperature the shape of the magnetization loops changes dramatically over the narrow temperature range of 5 K. Magnetization loops at temperatures higher than 7.75 K were also measured but no flux jumps were found. While

the magnetization loop at 7.75 K shows no flux jumps, solitary jumps appear at the slightly lower temperature of 7.55 K [Fig. 4(b)] where the jumps are almost complete ($M \simeq 0$). At 7.0 K the first jump in the virgin magnetization curve [Fig. 4(c)] occurs. No jump appears in a decreasing field between 5.5 and 0 T and a single jump shows up between 0 and −5.5 T. At 2.5 K [Fig. 4(e)] two jumps occur in the virgin curve and now there is a jump between 5.5 and 0 T in a decreasing field and three jumps are present between 0 and −5.5 T. The flux jumps are less complete at lower than at higher temperatures.

As one can see from the Appendix the magnetization in our model depends on four parameters which are (i) H^*, the field of full penetration where $H^* = -H_0 + \sqrt{H_0^2 + J_0 H_0 d}$, (ii) H_j^*, the field of full penetration at the maximum temperature the sample reaches during a flux jump where $H_j^* < H^*$,

$$H_j^* = -H_0 + \sqrt{H_0^2 + J_{0j} H_0 d} \ ,$$

and J_{0j} is the critical current density in zero field at that maximum temperature, (iii) H_0, the phenomenological parameter in the expression for J_c [Eq. (1)], and (iv) H_{j0} the Bean-type instability field [Eq. (14)] which depends on T, T_c, and the specific heat C_v.

Figures 5(a)–5(e) show the calculated magnetization loops which correspond to the measured loops in Figs. 4(a)–4(e). Some formulas for the magnetization M are given in the Appendix. Because the temperature range of interest (2.5–7.5 K) is small compared to $T_c = 92$ K, and H^* and H_j^* decrease approximately linearly with temperature, the same values for H^* and H_j^* ($\mu_0 H^* = 5.5$ T, $\mu_0 H_j^* = 1$ T) were used for all five calculated loops in Figs. 5(a)–5(e). For H_0 a value of $\mu_0 H_0 = 4$ T was chosen. The parameter which changes most rapidly with

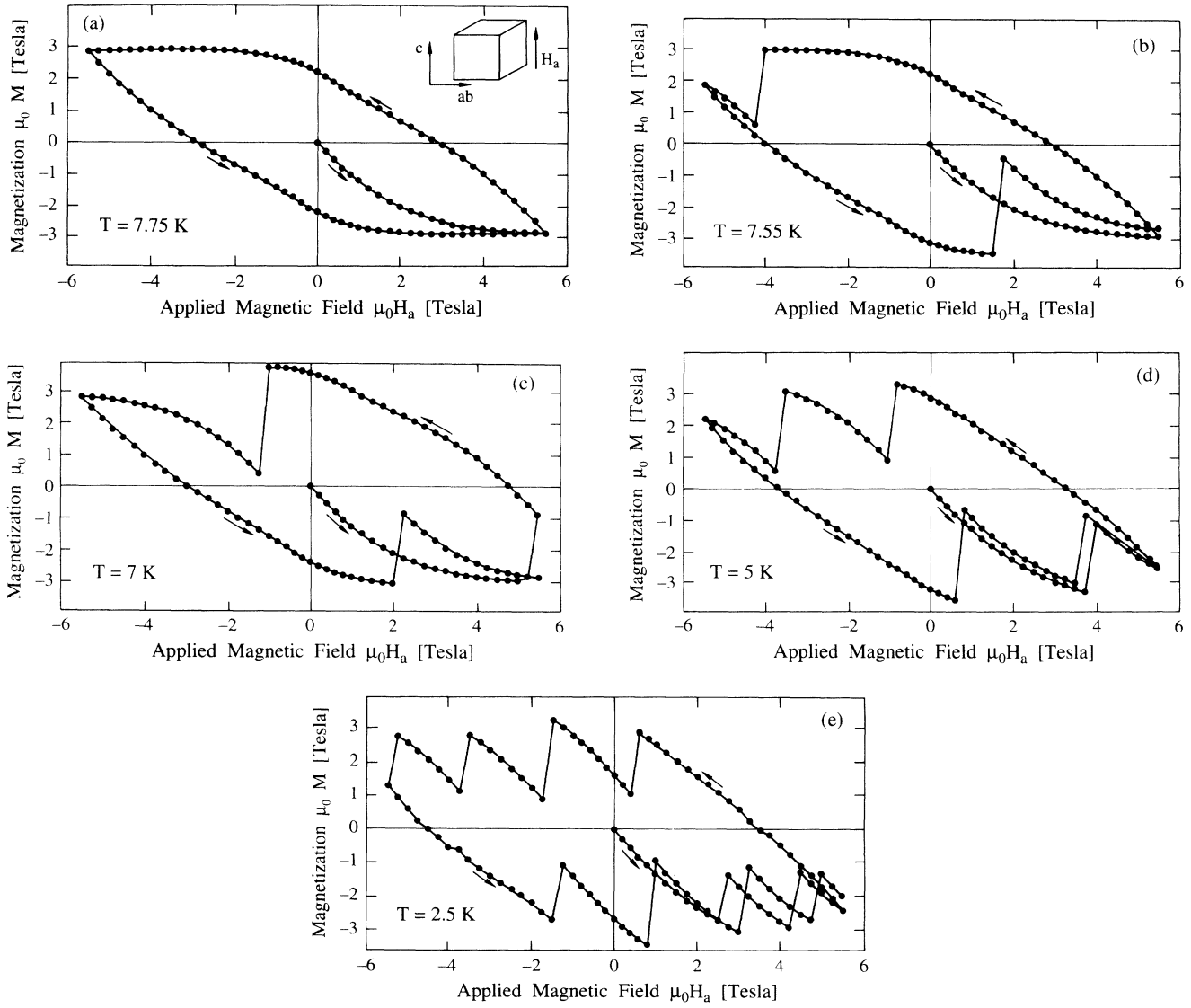

FIG. 4. Measured magnetization M as a function of the applied field H_a for the melt-textured Y-Ba-Cu-O sample at temperatures between 2.5 and 7.75 K. The magnetic field was applied parallel to the c axis.

temperature and most strongly affects the shape of the magnetization loop is H_{j0} [Eq. (14)]. The values of H_{j0} in Figs. 5(a)–5(e) were chosen to fit the experimental data. It is of importance to mention here that the loop in Fig. 5(b) (solitary jumps) and the loop in Fig. 5(c) cannot be produced using a critical-state model with a field-independent critical current density J_c (Bean critical state). This becomes clear if one constructs the magnetic-field profiles which, in the case of a field-independent J_c, consist of straight lines. In this case it is easy to realize that, if there is no jump in the virgin magnetization up to the maximum field H_m no jump is possible when the field is swept from H_m to the largest negative field $-|H_m|$. In addition, the simple Bean critical state model, even in the presence of flux jumps, predicts that the magnetization exhibits the symmetry $M(H) = -M(-H)$. A model with a monotonically decreasing $J_c(H)$ like ours, does not possess such a symmetry in the presence of jumps (Fig. 5) in agreement with the experimental data (Fig. 4).

When the field is applied parallel to the c axis, the field of full penetration H^* is determined by the critical current density, J_c^{ab}, flowing in the crystallographic ab-plane of the material and

$$H^* = -H_0 + \sqrt{H_0^2 + J_0 H_0 a_x/2}\ ,$$

where $J_0 = J_c^{ab}(H=0)$ and a_x is the width of our cubelike sample. Because of the square cross section of the sample, the magnetization M_{cube} at saturation is smaller than the magnetization M_{slab}, of a slab of thickness $d = a_x$. When the magnetization reaches saturation (i.e., $H_a > H^*$ for the virgin magnetization, $H_a < H_m - 2H^*$ in the upper branch or $H_a > -|H_m| + 2H^*$ in the lower branch

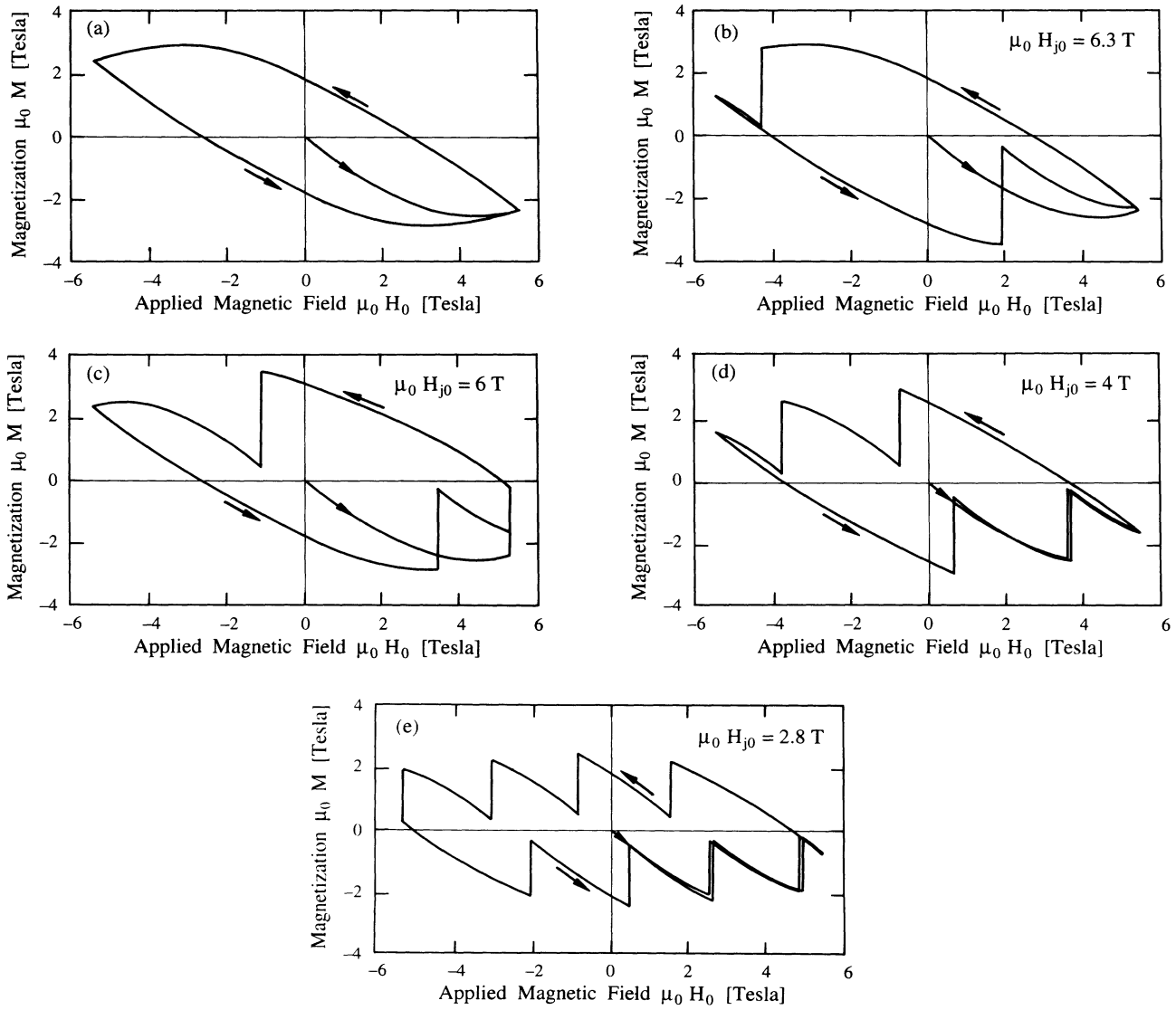

FIG. 5. Calculated magnetization M as a function of the applied field H_a. (a)–(e) correspond to the measured magnetization shown in Figs. 4(a)–4(e). The value of the parameter $\mu_0 H_{j0}$ is shown. The other parameters are $\mu_0 H^* = 5.5$ T, $\mu_0 H_j^* = 1$ T, and $\mu_0 H_0 = 4$ T.

of the loop), $M_{\text{cube}} = 2M_{\text{slab}}/3$ in the Bean model approximation.

The main effects of H^* on the magnetization loop are (i) the larger H^* the less rapidly the magnetization increases (decreases) when the applied field is decreased from H_m (increased from $-|H_m|$), and (ii) the larger H^* the larger the saturation magnetization becomes. The main effect of H_0 on the loop is that it produces maxima in $|M|$ at $H_a \simeq -H_0/2$ in the upper and at $H_a \simeq H_0/2$ in the lower branch of the magnetization. The maxima become more pronounced with decreasing H_0.

The expressions for the magnetization M given in the Appendix scale with H^* and thus one can predict the range of the reduced parameters H_{j0}/H^* and H_0/H^* for which at fixed H_m/H^* (i) no jump, (ii) solitary jumps, and (iii) one or several virgin jumps occur. Jumps in the virgin magnetization curve appear for $H_m \leq H^*$ if $H_{fi} \leq H_m$. In contrast, if $H_m > H^*$, a jump in the virgin magnetization can only be observed if $H_{fi} \leq H^*$ and no jump will show up in the field range $H^* \leq H_a \leq H_m$. Figure 6 shows different regions in the H_{j0}/H^* versus H_0/H^* diagram for $H_m/H^* = 1$. The parameter range where solitary flux jumps occur is small compared to the range where jumps in the virgin magnetization curve (and in the magnetization loop) appear. The temperature range (H_{j0} range) over which solitary jumps exist decreases with increasing H_0/H^* and vanishes in the limit $H_0/H^* \to \infty$ (Bean critical state).

Figures 7(a)–7(d) show the measured magnetization loops at temperatures between 1.75 and 3.9 K, where now the external field is applied perpendicular to the crystallographic c axis of the melt-textured Y-Ba-Cu-O sample. Magnetization loops at temperatures higher than 3.9 K were also measured but did not show any flux jumps. Solitary jumps were found in the vicinity of 3.5 K [Fig. 7(b)]. At 3.0 K [Fig. 7(c)] a single flux jump appears in the virgin magnetization and no jump is to be seen in a decreasing field between 5.5 and 0 T while two jumps appear between 0 and -5.5 T. At the lowest temperature of 1.75 K two flux jumps are seen in the virgin magnetization. A single jump now also appears in a decreasing positive field and several jumps occur in an increasing negative field between 0 and -5.5 T. The flux jumps in Fig. 7 are less complete than in Fig. 5 and in contrast to Fig. 5 the loops now show $M(H) = -M(-H)$ symmetry.

The calculated magnetization loops which correspond to Figs. 7(a)–7(d) are shown in Figs. 8(a)–8(d). Good fits to the experimental data were obtained with $\mu_0 H^* = 2.2$ T, $\mu_0 H_j^* = 1.14$ T, $\mu_0 H_0 = 8$ T, and the values for $\mu_0 H_{j0}$

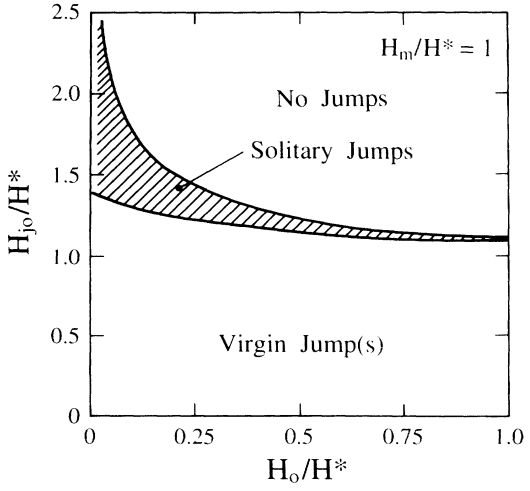

FIG. 6. Diagram of H_{j0}/H^* versus H_0/H^* for $H_m/H^* = 1$ with regions where no jumps, solitary jumps, and jumps in the virgin magnetization occur.

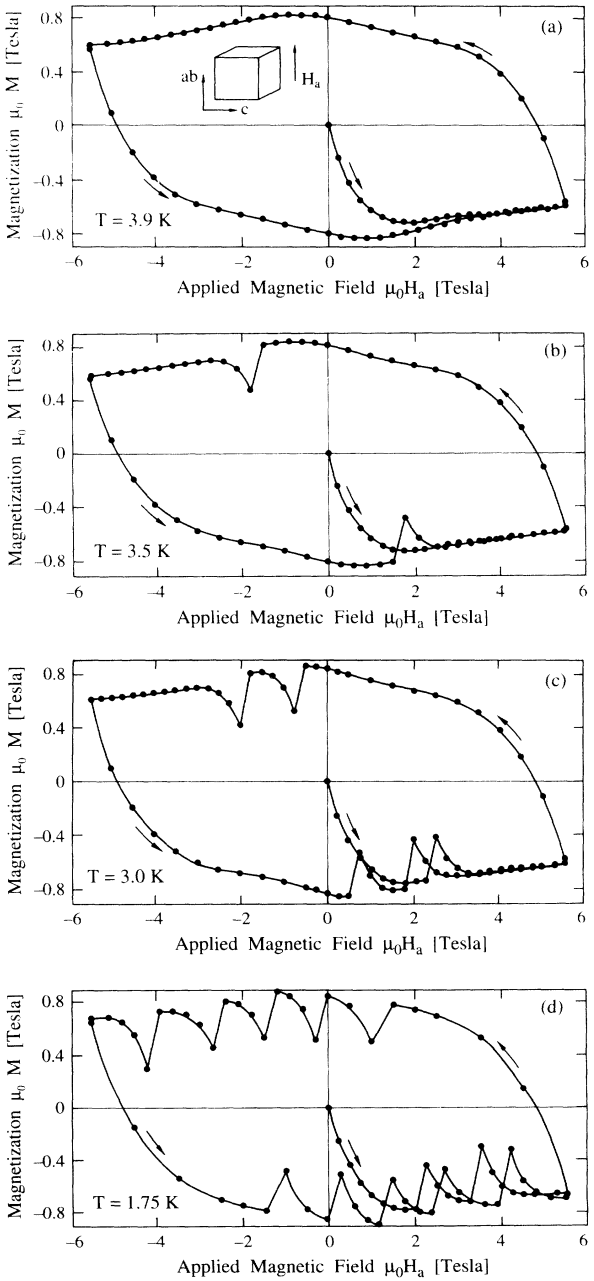

FIG. 7. Measured magnetization M as a function of the applied field H_a for the melt-textured Y-Ba-Cu-O sample at temperatures between 1.75 and 3.9 K. The magnetic field was applied perpendicular to the c axis.

shown in Figs. 8(b)–8(d). The essential difference between Figs. 8 and 5 is that now the value of H^* is smaller by about a factor of 2 because of the smaller critical current density J_c^c in c direction compared to J_c^{ab} along the ab plane. Another essential difference is that now the virgin instability (jump) field, H_{fi1}^V, is not limited by H_m but instead by H^*. Closely related to this is the nonexistence of further flux jumps in the upper branch of the magnetization loop below -2.5 T in Fig. 8(c) (flat region), due to the fact that the critical current density weakens in a strong field causing the penetrating flux fronts to meet in the center of the sample before a jump instability can occur. This is also the reason for the $M(H)=-M(-H)$ symmetry in Figs. 7 and 8 where the penetrating flux fronts completely wipe out any memory of previous flux jumps in contrast to the asymmetric loops in Figs. 4 and 5.

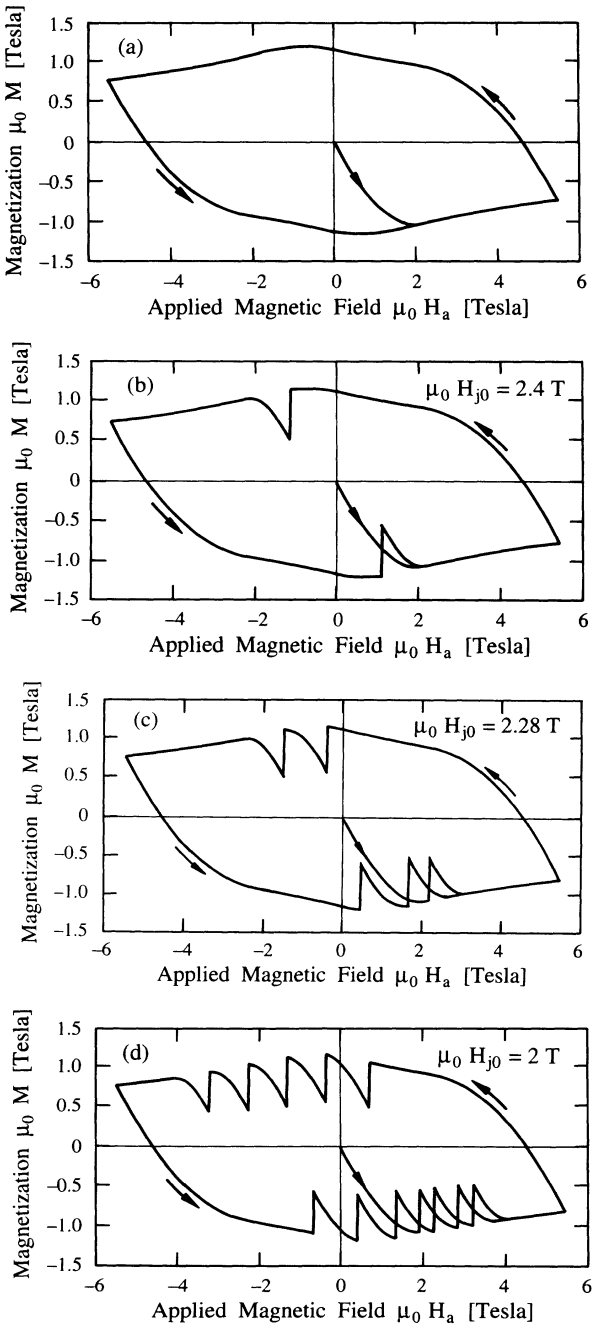

FIG. 8. Calculated magnetization M as a function of the applied field H_a. (a)–(d) correspond to the measured magnetization shown in Figs. 7(a)–7(d). The value of the parameter $\mu_0 H_{j0}$ is shown. The other parameters are $\mu_0 H^* = 2.2$ T, $\mu_0 H_j^* = 1.14$ T, and $\mu_0 H_0 = 8$ T.

When the field is applied perpendicular to the c axis of the cubelike sample, two different expressions for H^* are involved[27] (see Fig. 9). Because $J_c^{ab} \gg J_c^c$ the magnetic-field distribution in a cubelike sample resembles that of a slab if one neglects the short portions where the current flows along the ab plane as indicated in Fig. 9. The magnetic behavior of such a cubelike sample is very similar to that of a slab, i.e., $M_{\text{cube}} \simeq M_{\text{slab}}$, where the field of full penetration is

$$H^* = -H_0 + \sqrt{H_0^2 + J_0 H_0 a_x/2}$$

with $J_0 = J_c^c(H=0)$.

Figure 10 shows the virgin magnetization curves for the applied field perpendicular to the crystallographic c axis for the melt-textured Y-Ba-Cu-O sample at different temperatures. With increasing temperature the first virgin instability field, H_{fi1}^V, increases as expected from Eq. (13) because $C_v(T)$ increases with temperature. Above 3.05 K the virgin flux jump suddenly disappears indicating that at this temperature $H_{fi} > H^*$ and no jump instability can develop at higher temperatures.

From the different H^* values, which were used in the calculations to reproduce the measured magnetization loops in Figs. 4 and 7 for the two different orientations of the sample, one can roughly estimate the anisotropy of the current densities, J_c^{ab} and J_c^c. One finds that in zero field $J_c^{ab}/J_c^c \simeq 2.6$. Using the Bean-model saturation

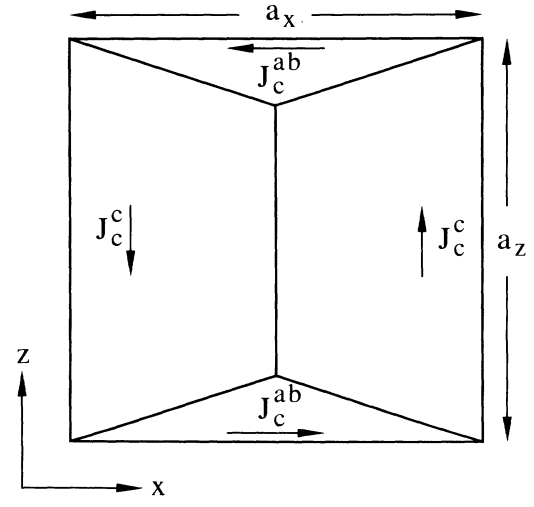

FIG. 9. Top view of the magnetic field distribution inside the sample where the field is applied perpendicular to the x-z plane, i.e., perpendicular to the crystallographic c axis. Because $J_c^{ab} \gg J_c^c$, the field distribution is mainly due to the current J_c^c flowing in c direction.

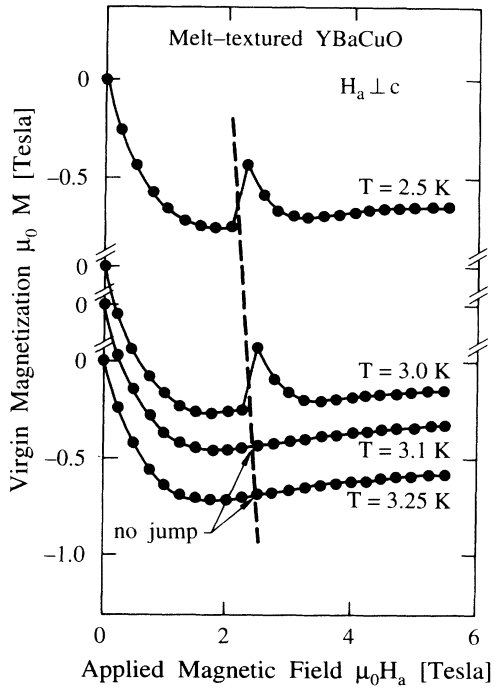

FIG. 10. Virgin magnetization versus applied magnetic field at different temperatures. The virgin jump disappears above 3.05 K.

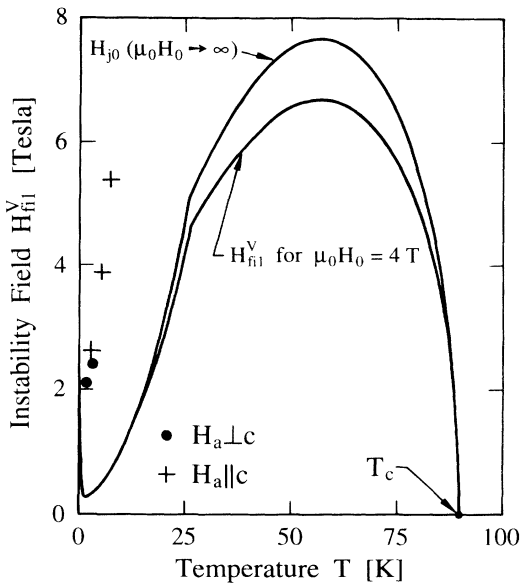

FIG. 11. Measured and calculated first virgin instability field H_{fi1}^V as a function of temperature. The calculated instability field H_{fi1}^V decreases with decreasing H_0.

magnetizations $M_{\text{cube}} = J_c^{ab} a_x/6$ for $H_a \| c$ and $M_{\text{cube}} \simeq M_{\text{slab}} = J_c^c a_x/4$ for $H_a \perp c$, one finds from Figs. 5(a) and 7(a) the ratio $J_c^{ab}/J_c^c \simeq 5.5$.

The values for H_{j0}, which determine the jumps in Figs. 5(b)–5(e) and Figs. 8(b)–8(d), were chosen to fit the experimental data. If one uses instead Eq. (14) to calculate H_{j0} (which is H_{fi} in the limit of $H_0 \to \infty$) and compares the result with the experimentally found first jump field, H_{fi1}^V, of the virgin magnetization, one finds a large discrepancy between both as illustrated in Fig. 11. Here, H_{j0} is much smaller than H_{fi1}^V. The discrepancy remains if the first virgin instability field H_{fi1}^V is calculated using Eq. (13) with $\mu_0 H_0 = 4$ T and $H_e = 0$. A finite H_0 reduces H_{fi}, though for $\mu_0 H_0 = 4$ T the effect is negligible below 10 K. The deflection in the calculated curve at about 26 K is due to the different sets of parameters used to fit the experimental $C_v(T)$ data of Y-Ba-Cu-O below and above 26 K. Expressions for $C_v(T)$ were taken from Ref. 18 where

$$C_v(1\text{–}26\ \text{K})\ ,\ \text{J cm}^{-3}\ :$$

$$2.6868\times10^{-4}\ \text{T}^{-2} + 1.0135\times10^{-4}\ \text{T} + 2.5338\times10^{-6}\ \text{T}^3 + 7.1712\times10^{-9}\ \text{T}^5$$

and

$$C_v(26\text{–}100\ \text{K})\ ,\ \text{J cm}^{-3}\ :$$

$$2.0228\times10^{-4}\ \text{T}^2 - 7.8163\times10^{-9}\ \text{T}^4\ .$$

The discrepancy between experiment and calculation in Fig. 11 is believed to be due to the dependence of H_{fi} on the sweep rate of the applied field H_a which has been discussed recently by Gerber, Taranawski, and Fanse.[28] A sweep rate dependence has not been considered in the derivation of Eq. (14) for H_{fi}.

For our low sweep rate of 1.2 T/min one can expect that a larger applied magnetic field is needed for the initialization of a jump to compensate for the flow of heat into the surrounding helium gas of the magnetometer. If one wants to check the predictions of Eqs. (13) and (14) for the first virgin instability field the sample should be better isolated thermally and the jump should be initiated by a small magnetic field superimposed on the applied field causing a sudden small change ΔH_a.[29]

V. CONCLUSIONS

The magnetization loops of a cubelike melt-textured Y-Ba-Cu-O sample were measured using a SQUID magnetometer in the applied magnetic-field range between −5.5 and 5.5 T. For a field applied parallel to the crystallographic c axis of the sample, flux jumps were observed at temperatures below 7.6 K. For an applied field perpendicular to the c axis the appearance of jumps was suppressed by the small size of the sample and the weak current along the c axis, and flux jumps only started to appear at temperatures below 3.5 K. The shape of the magnetization loop with its flux jumps could be calculated in detail as a function of temperature employing a critical state model which takes into account the flux jump instability criterion. In order to understand the occurrence of solitary flux jumps and the asymmetry between upper and lower magnetization branches, a field-dependent critical density is required in the critical-state model. The assumption that the critical-state field profile, formed during the jump, is frozen-in after the completion of a jump, leads to an excellent description of

the magnetization loops which contain partial jumps. The commonly used expression for the instability field failed to predict the first virgin instability field because the heat exchange between sample and coolant is neglected. The ratio J_c^{ab}/J_c^c could be estimated from the different H^* values and from the saturation of the magnetization.

ACKNOWLEDGMENTS

The authors would like to thank H. T. Ren, J. A. Xia, and S. X. Dou from the School of Materials Science and Engineering at the University of New South Wales in Sydney, Australia, for providing the high-quality melt-textured Y-Ba-Cu-O sample.

APPENDIX

This appendix deals with magnetization loops which contain solitary flux jumps, i.e., no jump in the virgin magnetization and only one jump in the upper and one in the lower branch of the magnetization loop.

(a) For an increasing positive applied field H_a, where $0 \le H_a \le H_m$, the virgin magnetization M for a slab of thickness d is given by

$$M = -H_0 \frac{\alpha_{11}}{d} - \frac{2}{3J_0H_0d}\{[(H_0+H_a)^2 - 2J_0H_0\alpha_{11}]^{3/2} - (H_0+H_a)^3\} - H_a \ , \tag{A1}$$

where α_{ij}, $i=1,2,\ldots$; $j=1,2,\ldots$ is defined as

$$\alpha_{ij}/d = \begin{cases} x_{ij}/d & \text{if } x_{ij}/d < \frac{1}{2} \\ \frac{1}{2} & \text{otherwise} \ . \end{cases} \tag{A2}$$

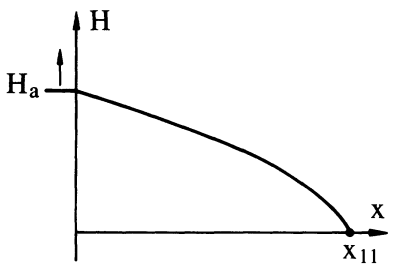

FIG. 12. Virgin magnetic-field profile $H(x)$ in a semi-infinite slab.

Here

$$\frac{x_{11}}{d} = \frac{(H_0+H_a)^2 - H_0^2}{2J_0H_0d} \quad \text{(see Fig. 12)} \tag{A3}$$

with

$$J_0H_0d = (H^*)^2 + 2H_0H^* \ , \tag{A4}$$

where H^* is the field of full penetration. (A flux jump in the virgin magnetization cannot be observed if the instability field H_{fi} of Eq. (13) where

$$H_e = -H_0 + [(H_0+H_a)^2 - 2J_0H_0\alpha_{11}]^{1/2}$$

is greater than the maximum applied field H_m or greater than the field of full penetration H^*.)

(b) For a decreasing positive applied field H_a where $0 \le H_a \le H_m$:

$$M = -2H_0\frac{\alpha_{11}}{d} + \frac{2}{3J_0H_0d}\{[(H_0+H_a)^2 + 2J_0H_0\alpha_{12}]^{3/2} - (H_0+H_a)^3\} - \frac{2}{3J_0H_0d}\{[(H_0+H_m)^2 - 2J_0H_0\tilde{\alpha}_{11}]^{3/2} - [(H_0+H_m)^2 - 2J_0H_0\alpha_{12}]^{3/2}\} - H_a \ , \tag{A5}$$

where

$$\frac{x_{12}}{d} = \frac{(H_0+H_m)^2 - (H_0+H_a)^2}{4J_0H_0d} \quad \text{(see Fig. 13)} \tag{A6}$$

and

$$\tilde{\alpha}_{11} = \alpha_{11}|_{H_a=H_m} \ . \tag{A7}$$

It follows from Eqs. (13) and (19) that if no jump exists in the virgin magnetization, no jump can occur when the applied field is decreased from H_m to 0.

(c) For an increasing negative applied field H_a, where $H_{fi1} \le H_a \le 0$ (H_{fi1} is the first instability field):

$$M = 4H_0\frac{\alpha_{13}}{d} - 2H_0\frac{\tilde{\alpha}_{11}}{d} + \frac{2}{3J_0H_0d}\{[(H_0-H_a)^2 - 2J_0H_0\alpha_{13}]^{3/2} - (H_0-H_a)^3\} + \frac{2}{3J_0H_0d}\{[(H_0^2 + 2J_0H_0(\alpha_{14}-\alpha_{13})^{3/2} - H_0^3\} - \frac{2}{3J_0H_0d}\{[(H_0+H_m)^2 - 2J_0H_0\tilde{\alpha}_{11}]^{3/2} - [(H_0+H_m)^2 - 2J_0H_0\alpha_{14}]^{3/2}\} - H_a \ , \tag{A8}$$

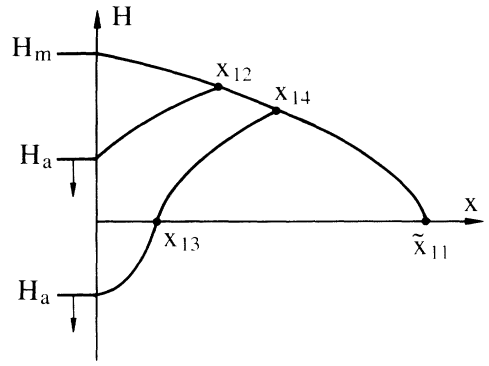

FIG. 13. Magnetic-field profiles $H(x)$ in a semi-infinite slab for a decreasing positive and an increasing negative applied field H_a.

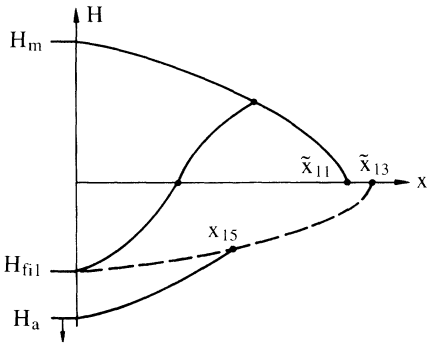

FIG. 14. Magnetic-field profiles $H(x)$ in a semi-infinite slab for an increasing negative applied field H_a. A flux jump occurs at $H_a = H_{fi1}$.

where

$$\frac{x_{13}}{d} = \frac{(H_0 - H_a)^2 - H_0^2}{2J_0 H_0 d} \quad \text{(see Fig. 13)} \tag{A9}$$

and

$$\frac{x_{14}}{d} = \frac{2H_0 H_m + H_m^2}{4J_0 H_0 d} + \frac{x_{13}}{2d} \quad \text{(see Fig. 13)} . \tag{A10}$$

The instability field H_{fi1}, is given by solving Eq. (19) where

$$H_e = -H_0 + \sqrt{H_0^2 + 2J_0 H_0 (\alpha_{14} - \alpha_{13})} \tag{A11}$$

if $x_{13}/d < \frac{1}{2}$ and otherwise by Eq. (13) where

$$H_e = H_0 - \sqrt{(H_0 - H_a)^2 - 2J_0 H_0 \alpha_{13}} . \tag{A12}$$

During a flux jump the temperature inside the sample increases and reaches a maximum temperature T^* which is assumed to be approximately independent of the position x inside the sample. The critical current density at T^* is denoted by J_{0j} where $J_{0j} < J_0$. During the jump the magnetic-field distribution $H(x)$ changes to a profile according to J_{0j} which is frozen-in when the sample temperature drops back to the bath temperature T. For our experimental magnetization loops with solitary jumps, one finds that $\tilde{\alpha}_{13} \geq \tilde{\alpha}_{11}$ (see Fig. 14) and thus the case $\tilde{\alpha}_{13} \leq \tilde{\alpha}_{11}$ will not be considered here.

(d) For an increasing negative applied field H_a, where $-|H_m| \leq H_a \leq H_{fi1}$:

$$M = 2H_0 \frac{\tilde{\alpha}_{13}}{d} + \frac{2}{3J_0 H_0 d}\{[(H_0 - H_a)^2 - 2J_0 H_0 \alpha_{15}]^{3/2} - (H_0 - H_a)^3\}$$
$$+ \frac{2}{3J_{0j} H_0 d}\{[(H_0 - H_{fi1})^2 - 2J_{0j} H_0 \tilde{\alpha}_{13}]^{3/2} - [(H_0 - H_{fi1})^2 - 2J_{0j} H_0 \alpha_{15}]^{3/2}\} - H_a , \tag{A13}$$

where

$$\frac{x_{15}}{d} = \frac{(H_0 - H_{fi1})^2 - (H_0 - H_a)^2}{2H_0 d(J_{0j} - J_0)} \quad \text{(see Fig. 14)} \tag{A14}$$

and

$$\frac{\tilde{x}_{13}}{d} = \frac{(H_0 - H_{fi1})^2 - H_0^2}{2J_{0j} H_0 d} \quad \text{(see Fig. 14)} . \tag{A15}$$

Here $J_{0j} H_0 d = (H_j^*)^2 + 2H_0 H_j^*$ where H_j^* is the field of full penetration during the jump process when the maximum temperature T^* has been reached.

(e) For a decreasing negative applied field H_a, where $-|H_m| \leq H_a \leq 0$ we have the following.

(1) If $x_{16} \leq \tilde{x}_{15}$ (see Fig. 15) then

$$M = 2H_0 \frac{\tilde{\alpha}_{13}}{d} - \frac{2}{3J_0 H_0 d}\{[(H_0 - H_a)^2 + 2J_0 H_0 \alpha_{16}]^{3/2} - (H_0 - H_a)^3\}$$
$$+ \frac{2}{3J_0 H_0 d}\{[(H_0 - H_m)^2 - 2J_0 H_0 \tilde{\alpha}_{15}]^{3/2} - [(H_0 - H_m)^2 - 2J_0 H_0 \alpha_{16}]^{3/2}\}$$
$$+ \frac{2}{3J_{0j} H_0 d}\{[(H_0 - H_{fi1})^2 - 2J_{0j} H_0 \tilde{\alpha}_{13}]^{3/2} - [(H_0 - H_{fi1})^2 - 2J_{0j} H_0 \tilde{\alpha}_{15}]^{3/2}\} - H_a , \tag{A16}$$

where

$$\tilde{\alpha}_{15} = \alpha_{15}|_{H_a = H_m} \quad \text{(see Fig. 15)} \tag{A17}$$

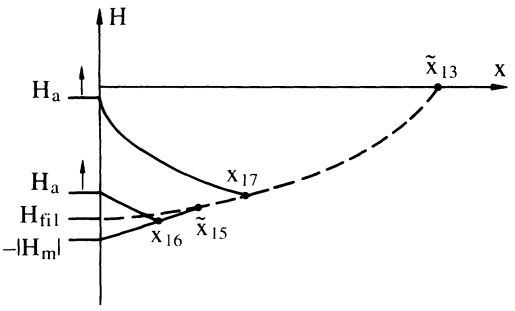

FIG. 15. Magnetic-field profiles $H(x)$ in a semi-infinite slab for a decreasing negative applied field, H_a.

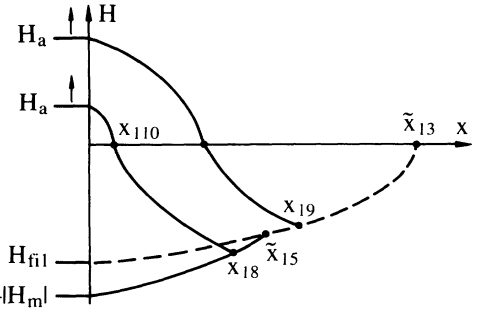

FIG. 16. Magnetic-field profiles $H(x)$ in a semi-infinite slab for an increasing positive applied field H_a.

and

$$\frac{x_{16}}{d}=\frac{(H_0-H_m)^2-(H_0-H_a)^2}{4J_0H_0d}\text{(see Fig. 15)} . \tag{A18}$$

(2) If $x_{16}>\tilde{x}_{15}$ (see Fig. 15) then

$$M=2H_0\frac{\tilde{\alpha}_{13}}{d}-\frac{2}{3J_0H_0d}\{[(H_0-H_a)^2+2J_0H_0\alpha_{17}]^{3/2}-(H_0-H_a)^3\}$$
$$+\frac{2}{3J_{0j}H_0d}\{[(H_0-H_{fi1})^2-2J_{oj}H_0\tilde{\alpha}_{13}]^{3/2}-[(H_0-H_{fi1})^2-2J_{0j}H_0\alpha_{17}]^{3/2}\}-H_a , \tag{A19}$$

where

$$\frac{x_{17}}{d}=\frac{(H_0-H_{fi1})^2-(H_0-H_a)^2}{2H_0d(J_{0j}+J_0)} \text{ (see Fig. 15)} . \tag{A20}$$

(f) For an increasing positive applied field H_a, where $0\le H_a\le H_{fi2}$ (H_{fi2} is the second instability field) we have the following.

(1) If $x_{18}\le\tilde{x}_{15}$ (see Fig. 16) then

$$M=-4H_0\frac{\alpha_{110}}{d}+2H_0\frac{\tilde{\alpha}_{13}}{d}-\frac{2}{3J_0H_0d}\{[(H_0+H_a)^2-2J_0H_0\alpha_{110}]^{3/2}-(H_0+H_a)^3\}$$
$$-\frac{2}{3J_0H_0d}\{[H_0^2+2J_0H_0(\alpha_{18}-\alpha_{110})]^{3/2}-H_0^3\}$$
$$+\frac{2}{3J_0H_0d}\{[(H_0-H_m)^2-2J_0H_0\tilde{\alpha}_{15}]^{3/2}-[(H_0-H_m)^2-2J_0H_0\alpha_{18}]^{3/2}\}$$
$$+\frac{2}{3J_{0j}H_0d}\{[(H_0-H_{fi1})^2-2J_{0j}H_0\tilde{\alpha}_{13}]^{3/2}-[(H_0-H_{fi1})^2-2J_{0j}H_0\tilde{\alpha}_{15}]^{3/2}\}-H_a , \tag{A21}$$

where

$$\frac{x_{110}}{d}=\frac{(H_0+H_a)^2-H_0^2}{2J_0H_0d} \text{ (see Fig. 16)} \tag{A22}$$

and

$$\frac{x_{18}}{d}=\frac{(H_0-H_m)^2-H_0^2+2J_0H_0x_{110}}{4J_0H_0d} \text{ (see Fig. 16)} . \tag{A23}$$

[In α_{110} and x_{110} the subscripts are $i=1$ and $j=10$ according to the definition of α_{ij} in Eq. (A2).] The flux jump at $H_a=H_{fi2}$ is determined by Eq. (19) where

$$H_e=H_0-\sqrt{H_0^2+2J_0H_0(\alpha_{18}-\alpha_{110})} \tag{A24}$$

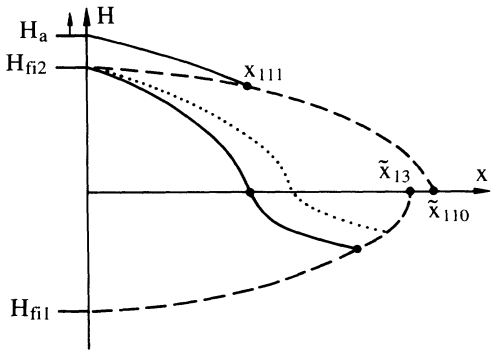

FIG. 17. Magnetic-field profiles, $H(x)$ in a semi-infinite slab for an increasing positive applied field H_a. A flux jump occurs at $H_a=H_{fi2}$.

if $x_{110}/d \leq 1/2$ and otherwise by Eq. (13) where

$$H_e = -H_0 + \sqrt{(H_0+H_a)^2 - 2J_0H_0\alpha_{110}} \ . \tag{A25}$$

(2) If $x_{18} > \tilde{x}_{15}$ then

$$M = -4H_0\frac{\alpha_{110}}{d} + 2H_0\frac{\tilde{\alpha}_{13}}{d} - \frac{2}{3J_0H_0d}\{[(H_0+H_a)^2 - 2J_0H_0\alpha_{110}]^{3/2} - (H_0+H_a)^3\}$$
$$- \frac{2}{3J_0H_0d}\{[H_0^2 + 2J_0H_0(\alpha_{19}-\alpha_{110})]^{3/2} - H_0^3\}$$
$$+ \frac{2}{3J_0H_0d}\{[(H_0-H_{fi1})^2 - 2J_{0j}H_0\tilde{\alpha}_{13}]^{3/2} - [(H_0-H_{fi1})^2 - 2J_{0j}H_0\alpha_{19}]^{3/2}\} - H_a \ , \tag{A26}$$

where

$$\frac{x_{19}}{d} = \frac{(H_0-H_{fi1})^2 - H_0^2 + 2J_0H_0x_{110}}{2H_0d(J_{0j}+J_0)} \quad \text{(see Fig. 16)} \ . \tag{A27}$$

The flux jump at $H_a = H_{fi2}$ is determined by Eq. (19) where

$$H_e = H_0 - \sqrt{H_0^2 + 2J_0H_0(\alpha_{19}-\alpha_{110})} \tag{A28}$$

if $x_{110}/d \leq 1/2$ and otherwise by Eq. (13) where H_e is given by Eq. (A25).

The different types of field profiles that might evolve after a jump are shown in Fig. 17 (dotted curve and upper dashed curve). Only the jump where $\tilde{x}_{110} > \tilde{x}_{13}$ (see Fig. 17) was needed to describe the experimental data in Figs. 4(b) and 8(b), and therefore only this case is discussed here.

(g) For an increasing positive applied field, H_a, where $H_{fi2} \leq H_a \leq H_m$:

$$M = -2H_0\frac{\tilde{\alpha}_{110}}{d} - \frac{2}{3J_0H_0d}\{[(H_0+H_a)^2 - 2J_0H_0\alpha_{111}]^{3/2} - (H_0+H_a)^3\}$$
$$- \frac{2}{3J_{0j}H_0d}\{[(H_0+H_{fi2})^2 - 2J_{0j}H_0\tilde{\alpha}_{110}]^{3/2} - [(H_0+H_{fi2})^2 - 2J_{0j}H_0\alpha_{111}]^{3/2}\} - H_a \ , \tag{A29}$$

where

$$\frac{\tilde{x}_{110}}{d} = \frac{(H_0+H_{fi2})^2 - H_0^2}{2J_{0j}H_0d} \quad \text{(see Fig. 17)} \tag{A30}$$

and

$$\frac{x_{111}}{d} = \frac{(H_0+H_a)^2 - (H_0+H_{f12})^2}{2H_0(J_0-J_{0j})} \quad \text{(see Fig. 17)} \ . \tag{A31}$$

[1] S. L. Wipf, Phys. Rev. **161**, 404 (1967).
[2] P. S. Swartz and C. P. Bean, J. Appl. Phys. **39**, 4991 (1968).
[3] M. N. Wilson, *Superconducting Magnets* (Clarendon Press, Oxford, 1983).
[4] S. L. Wipf, Cryogenics **31**, 936 (1991).
[5] J. L. Tholence, H. Noel, J. C. Levet, M. Potel, and P. Gougeon, Solid State Commun. **65**, 1131 (1988).
[6] M. Guillot, M. Potel, P. Gougeon, H. Noel, J. C. Levet, G. Chouteau, and J. L. Tholence, Phys. Lett. A **127**, 363 (1988).
[7] J. L. Tholence, H. Noel, J. C. Levet, M. Potel, P. Gougeon, G. Chouteau, and M. Guillot, Physica C **153-155**, 1479 (1988).
[8] M. Guillot, J. L. Tholence, O. Laborde, M. Potel, P. Gougeon, H. Noel, and J. C. Levet, Physica C **162-164**, 361 (1989).
[9] K. Chen, S. W. Hsu, T. L. Chen, S. D. Lan, W. H. Lee, and P. T. Wu, Appl. Phys. Lett. **56**, 2675 (1990).
[10] K. Chen, Y. C. Chen, S. W. Lu, W. H. Lee, and P. T. Wu, Physica C **173**, 227 (1991).
[11] K. Watanabe, N. Kobayashi, S. Awaji, G. Kido, S. Nimori, K. Kimura, K. Sawano, and Y. Muto, Jpn. J. Appl. Phys. **30**, L1638 (1991).
[12] K. Watanabe, S. Awaji, N. Kobayashi, S. Nimori, G. Kido, K. Kimura, and M. Hashimoto, Cryogenics **32**, 959 (1992).
[13] T. Ogasawara, Cryogenics **29**, 3 (1989).
[14] T. Ogasawara, Cryogenics **29**, 6 (1989).
[15] Y. Iwasa, IEEE Trans. Magn. **MAG-24**, 1211 (1988).
[16] S. L. Wipf, in *Proceedings of the Twelfth International Cryogenic Engineering Conference, ICEC 12,* Southampton, United Kingdom, 1988, edited by R. G. Scurlock and C. A. Bailey (Butterworth, Guildford, United Kingdom, 1988), p. 931.
[17] H. L. Laquer, F. J. Edeskuty, W. V. Hassenzahl, and S. L. Wipf, IEEE Trans. Magn. **MAG-25**, 1516 (1989).
[18] E. W. Collings, in *Advances in Superconductivity II,* Proceedings of the ISS'89, edited by T. Ishiguro and K. Kajimura (Springer, Tokyo, Japan, 1990), p. 327.
[19] S. L. Wipf and H. L. Laquer, IEEE Trans. Magn. **MAG-25**, 1877 (1989).

[20]J. H. P. Watson, in *Proceedings of the Twelfth International Cryogenic Engineering Conference, ICEC 12* (Ref. 16), p. 988.
[21]S. Jin, T. H. Tiefel, R. C. Sherwood, R. B. van Dover, M. E. Davis, G. W. Kammlott, and R. A. Fastnacht, Phys. Rev. B **37**, 7850 (1988).
[22]Y. B. Kim, C. F. Hempstead, and A. R. Strnad, Phys. Rev. Lett. **9**, 306 (1962).
[23]C. Andrikidis, K.-H. Müller, N. Savvides, S. X. Dou, and H. K. Liu, Cryogenics **32**, 411 (1992).
[24]D. D. Stancil, T. E. Schlesinger, A. K. Stamper, and D. Wong, J. Appl. Phys. **64**, 5899 (1988).
[25]Y. Yeshurun, A. P. Malozemoff, F. Holzberg, and T. R. Dinger, Phys. Rev. B **38**, 11 828 (1988).
[26]J. E. C. Williams, *Superconductivity and its Applications* (Pion Limited, London, 1970).
[27]R. L. Peterson, J. Appl. Phys. **67**, 6930 (1990).
[28]A. Gerber, Z. Taranawski, and J. J. M. Fanse, Physics C **209**, 147 (1993).
[29]T. Akachi, T. Ogasawara, and K. Yasukochi, Jpn. J. Appl. Phys. **20**, 1559 (1981).